ELSEVIER

Journal of Fluids and Structures 25 (2009) 95–111

JOURNAL OF FLUIDS AND STRUCTURES

www.elsevier.com/locate/jfs

Time marching for simulation of fluid–structure interaction problems

E. Longatte[a,*], V. Verreman[a], M. Souli[b]

[a]*Fluid Mechanics, Energy and Environment Department, EDF R&D Division, 6 Quai Watier, 78400 Chatou, France*
[b]*Mechanical Engineering Department, Lille University, 1 Boulevard Paul Langevin, 59655 Lille, France*

Received 4 May 2006; accepted 18 March 2008
Available online 10 June 2008

Abstract

Numerical simulation of industrial multi-physics problems is still a challenge. It generally requires large computational resources. It may involve complex code coupling techniques. It also relies on appropriate numerical methods making data transfer possible, quick and accurate. In the framework of partitioned procedures, multi-physics computations require the right choice of code coupling schemes, because several physical mechanisms are involved. Numerical simulation of fluid–structure interactions is one of these issues. It is investigated in this paper. First the computational process involving a code coupling procedure is presented. Then, applications and test cases involving fluid structure interactions are investigated using several examples. A partitioned procedure involves several operators ensuring code coupling. A special attention must be paid to energy conservation at the fluid–structure interface, especially when it is moving and when strong non-linear behaviour occurs in both fluid and structure systems. In the present work, several fluid–structure code-coupling schemes are compared and discussed in terms of stability and energy conservation properties. The criteria are based on the evaluation of the energy that is numerically created at the fluid–structure interface. This is achieved by considering the staggering process due to the time lag between the fluid and structure solvers. Comparisons are made, and finally the article gives recommendations for creating a tool devoted to coupled simulations of fluid structure interactions.

Keywords: Fluid–structure interaction; Code coupling scheme; Tube vibration; Tube bundle

1. Introduction

Flow-induced vibration problems occur in many industrial devices causing possible damage and even failure when resonance or instability arises. For specific components like heat exchangers, semi-empirical correlations based on experimental data have been identified under specific conditions. However, additional numerical studies are required because of the complexity due to multi-physics phenomena involved. In the present paper the numerical simulation of flow-induced vibrations in mechanical components involving tubes and tube bundles is investigated. The purpose is to suggest a suitable numerical methodology and to apply it to academic configurations assumed to be relevant for testing numerical algorithms.

*Corresponding author.
E-mail address: elisabeth.longatte@edf.fr (E. Longatte).

0889-9746/$ - see front matter
doi:10.1016/j.jfluidstructs.2008.03.009

Nomenclature

A_1, A_2, A_3, A_4	constants (dimensionless)
A_s^n	structure acceleration at time t^n ($m\,s^{-2}$)
C_a	added damping ($kg\,s^{-1}$)
C_s	structure damping ($kg\,s^{-1}$)
D_t	current time step (s)
D	tube diameter (m)
D_e	external tube diameter (m)
e	eccentricity (m)
E_f^n, ΔE_f^n	energy, energy variation associated to fluid motion at time t^n (N m)
E_s^n, ΔE_s^n	energy, energy variation associated to structure motion at time t^n (N m)
f	vibration frequency (Hz)
f_c	vibration frequency in the presence of fluid–structure coupling (Hz)
f_s	structure vibration frequency in air (Hz)
F_f^n	fluid force at time t^n ($kg\,m\,s^{-2}$)
F_s^n	fluid force applied to the structure at time t^n ($kg\,m\,s^{-2}$)
K_s	structure stiffness ($kg\,s^{-2}$)
Ω_f^n	fluid domain (dimensionless)
L	reference length in tube direction (m)
M_a	added mass (kg)
M_s, M_1, M_2	structure mass (kg)
P	longitudinal tube bundle pitch (m)
P/D	tube bundle pitch ratio (dimensionless)
ρ	fluid density ($kg\,m^{-3}$)
St	Stokes number (dimensionless)
t	time (s)
V_0, $V_1(0)$, $V_2(0)$	initial fluid velocity ($m\,s^{-1}$)
V_m^n	fluid mesh velocity at time t^n ($m\,s^{-1}$)
V_s^n	structure velocity at time t^n ($m\,s^{-1}$)
X_m^n	fluid mesh displacement at time t^n (m)
X_s^n, X_s^{1n}, X_s^{2n}	structure displacement at time t^n (m)
X_0	displacement magnitude (m)
α_0, α_1, β, γ	scheme constants (dimensionless)
δ_s, δ_e	logarithmic decrement in air, in water (dimensionless)
ε	scheme convergence error threshold (dimensionless)
μ	fluid dynamic viscosity ($kg\,m^{-1}\,s^{-1}$)
ν	fluid cinematic viscosity ($m^2\,s^{-1}$)
ξ	vibration damping (dimensionless)

As far as multi-physics problems are concerned, several physical problems have to be solved at the same time. This can be done in several ways. In this paper the case of a fluid–structure interaction problem is considered. A first method consists in solving the fluid and structure equations in a single system with a monolithic algorithm. This is a strong coupling process ensuring the energy conservation of the full-coupled fluid–structure system. However, the approach is often difficult to set up for industrial purposes as it requires significant modifications in fluid and structure solvers in order to make them compatible from a numerical point of view. Moreover, for large industrial problems, a monolithic method is time consuming and it requires a large memory allocation. These difficulties can be overcome by using a partitioned procedure ensuring an external coupling solver of separated fluid and structure codes. This method is easier to set up and it allows independent model development in both fluid and structure solvers. This is a time advancement code coupling method and it is investigated in the present paper.

With this procedure, each time step is decomposed as follows. Firstly, the computation of fluid forces acting on the structure is deduced from the fluid dynamic problem; secondly, the estimation of structure displacement and velocity induced by these fluid forces are solved in the structure dynamic solver. Finally, the fluid domain is adjusted according to the structure wall motion. This approach has the advantage of being very flexible from a numerical point of view. As discussed in previous papers (Piperno, 1997), it is well known that the time order of this approach is generally lower than the orders of both fluid and structure time integration schemes. Its stability limits are more restrictive than those of fluid and structure solvers. For this reason several procedures have been developed to improve the efficiency of the coupling process in terms of time-accuracy, stability and energy conservation at the fluid–structure interface.

The partitioned procedure may rely on several kinds of explicit or implicit time coupling schemes. With explicit synchronous schemes, fluid and structure computations are staggered in time and, as a result, the energy conservation may be violated. Explicit asynchronous schemes (Farhat et al., 1995; Farhat and Lesoinne, 1997; Piperno, 1997) and implicit schemes (Hermann and Steindorf, 1999; Le Tallec and Mouro, 2001; Mani, 2003) have been introduced to ensure better energy conservation. The first part of this paper is devoted to the presentation of several explicit and implicit code coupling schemes. Their different properties are presented and results are compared to analytical solutions.

In the second part, several studies are presented dealing with well-known test cases. Considering the time advancement of the portioned procedure, the simplified configurations presented in this article are particularly pertinent. Their modelling is based on beams, and no data projection is required at the fluid–structure interface for the space data transfer between the solvers at each time step. Hence it is possible to use these configurations to focus on the properties of the time code coupling schemes. They involve one- or two-dimensional test cases with one or several tubes

in the presence of viscous or non-viscous fluid initially at rest in incompressible fields. Comparisons to available experimental, numerical and analytical data are presented (Chen, 1987; Sinyavskii et al., 1980; Morand and Ohayon, 1995; Rogers et al., 1984; Weaver and Abd-Rabbo, 1985).

Finally, the article gives concluding remarks about the efficiency of the partitioned procedure. This sort of numerical simulation of coupled problems opens up perspectives for use in other complex configurations.

2. Computational process

2.1. Partitioned procedure

2.1.1. Code coupling procedure

As previously mentioned, the fluid–structure code coupling procedure is based on a partitioned method. Each time step is made of three steps: firstly, the computation of fluid forces acting on the structure; secondly, the resolution of structure dynamic equations; finally, the fluid mesh updating. A fluid mesh displacement process like an Arbitrary Lagrangian Eulerian (ALE) formulation is involved (Hughes et al., 1981; Souli and Zolesio, 2001). Fig. 1 illustrates the numerical algorithm for coupling. In order to set up the time marching process, different integration schemes are considered. At the moving fluid–structure interface, it is necessary not to produce or dissipate energy in order to avoid numerical damping. A first-order explicit synchronous scheme is possible but it may produce or dissipate energy at the coupling interface. Other time integration schemes can be used, like high-order staggered explicit schemes or implicit schemes. They may be based on a step-by-step procedure using a fixed point or a Newton method to solve the nonlinearity due to the interaction.

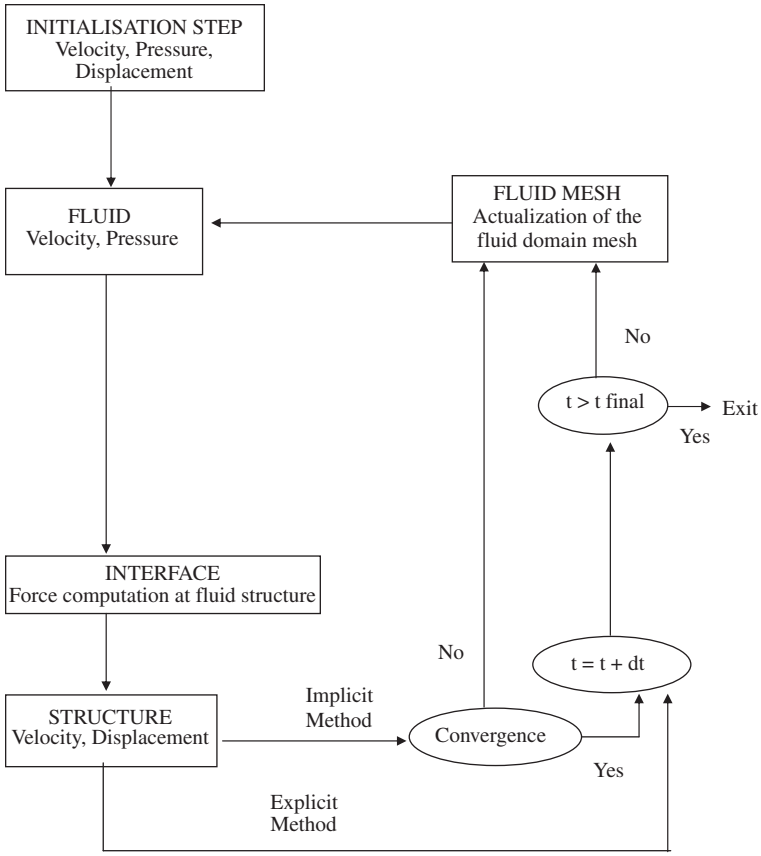

Fig. 1. Algorithm for the coupling of fluid and structure solvers with a partitioned procedure.

2.1.2. Fluid–structure interface

As previlously shown by Farhat et al. (1995), the loss in time accuracy and numerical stability of the partitioned procedure can lead to a violation of the energy conservation at the fluid–structure interface. The evaluation of the energy created by the coupling is considered below (Farhat et al., 1995; Piperno, 1997; Bendjeddou, 2005; Longatte et al., 2003; Piperno and Farhat, 2001). Both fluid and structure dynamics contribute to energy variation.

On one hand, the energy variation induced by the fluid computation at each time step can be expressed by the following equation:

$$\Delta E_f^{n+1} = -{}^T F_f^{n+1}(X_m^{n+1} - X_m^n). \tag{1}$$

${}^T F_f^{n+1}$ designates fluid forces acting on the structure estimated by the fluid solver at time t^{n+1}. X_m^n and X_m^{n+1} fluid are domain boundary displacements or boundary mesh displacements at times t^n and t^{n+1}.

On the other hand, the structure displacement can be modelled by using a classical structural dynamic equation of the form

$$M_s A_s^n + C_s V_s^n + K_s X_s^n = F_s^n, \tag{2}$$

where F_s^n designates forces acting on the structure at time t^n and A_s^n, V_s^n and X_s^n are, respectively, structure acceleration, velocity and displacement at time t^n.

The following development illustrates the energy variation measured by the structure computation. Eq. (2) is solved by using a Newmark algorithm for time integration:

$$M_s A_s^{n+1} + C_s V_s^{n+1} + K_s X_s^{n+1} = F_s^{n+1}. \tag{3}$$

Terms are estimated at first order as follows:

$$V_s^{n+1} = V_s^n + \frac{dt}{2}(A_s^n + A_s^{n+1}), \tag{4}$$

$$X_s^{n+1} = X_s^n + \frac{\Delta t}{2}(V_s^n + V_s^{n+1}) \tag{5}$$

with

$$V_s^{n+1/2} = \frac{V_s^{n+1} + V_s^n}{2} \quad \text{and} \quad X_s^{n+1/2} = \frac{X_s^{n+1} + X_s^n}{2}.$$

The energy of the structure is the sum of the kinetic and potential energies. Hence energy variation provided by structural computation between times t^n and t^{n+1} can be written as

$$\begin{aligned}\Delta E_s^{n+1} &= E_s^{n+1} - E_s^n = \tfrac{1}{2}{}^T(V_s^{n+1} + V_s^n)M_s(V_s^{n+1} - V_s^n) + \tfrac{1}{2}{}^T(X_s^{n+1} + X_s^n)K_s(X_s^{n+1} - X_s^n)\\ &= \Delta t^T\, V_s^{n+1/2}(M_s A_s^{n+1/2} + K_s X_s^{n+1/2}) = dt^T V_s^{n+1/2}(F_s^{n+1/2} - C_s V_s^{n+1/2}).\end{aligned} \tag{6}$$

Finally one gets

$$\Delta E_s^{n+1} = {}^T(X_s^{n+1} - X_s^n)\frac{F_s^{n+1} + F_s^n}{2} - dt^T V^{n+1/2} C_s V^{n+1/2}. \tag{7}$$

2.1.3. Interface conditions

The energy variation induced by the second term of Eq. (7) is due to the structure damping C_s. It does not account for energy variation generated by code-coupling. To reduce code-coupling errors and to ensure energy conservation at the interface, the following relationship must be satisfied:

$$\Delta E_s^{n+1} = (X_s^{n+1} - X_s^n)\frac{F_s^n + F_s^{n+1}}{2} = -{}^T F_f^n(X_m^{n+1} - X_m^n) = \Delta E_f^{n+1}. \tag{8}$$

Values of X_s^n and F_f^n are, respectively, the structural displacements and the fluid forces at the interface estimated by the codes. Code coupling schemes are based on this relation. The fluid mesh displacement X_m^n and the force F_s^n must be chosen to minimize this energy variation. In the following section, three explicit and implicit code coupling schemes are presented.

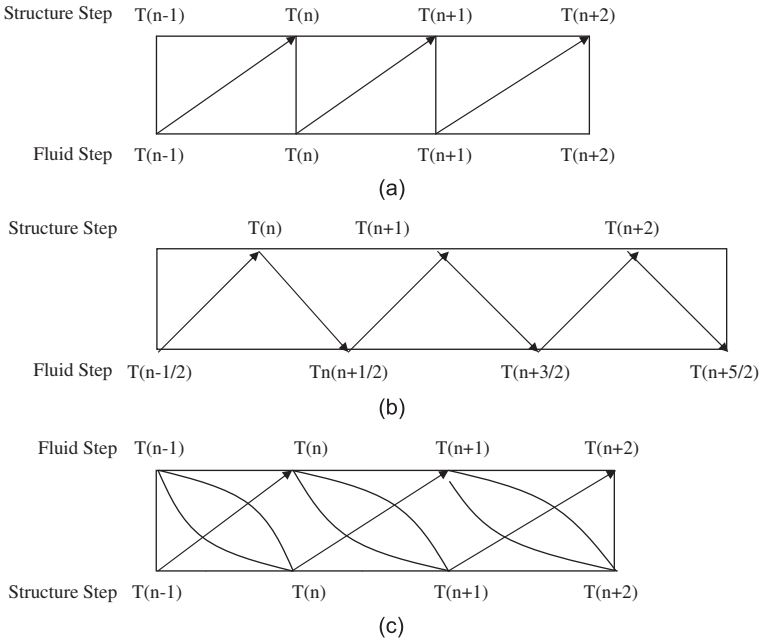

Fig. 2. Time advancement procedure with (a) an explicit synchronous code coupling scheme, (b) an explicit asynchronous code coupling scheme and (c) an implicit code coupling scheme.

2.2. Time integration schemes

2.2.1. Explicit synchronous algorithm (ESA)

With an explicit scheme, the structural displacement X_s^{n+1} at time t^{n+1} is deduced from the fluid force computation F_f^n at time t^{n+1} based on the fluid mesh position X_m at time t^{n+1} (Fig. 2(a)). A synchronous scheme gives a prediction of the fluid–structure interface position at time t^{n+1} by using previous positions known at times t^n and t^{n-1}. The following integration scheme is applied:

$$X_m^{n+1} = X_s^n + \alpha_0 \,\mathrm{d}t\, V_s^n + \alpha_1\, dt(V_s^n - V_s^{n-1}), \tag{9}$$

where X_s^n designates the structure displacement at time t^n, X_m^n the mesh displacement at time t^n, V^n and V^{n-1} the structure velocity at times t^n and t^{n-1}. The constants α_0 and α_1 are specific scheme coefficients and they are chosen according to the coupling process order.

Fluid forces F_s^{n+1} acting on the structure are calculated, structure displacement X_s^{n+1} is deduced from the mechanical equation. Constant α_0 and α_1 are chosen to get a high-order accuracy in the code coupling scheme. For $\alpha_0 = 1$ and $\alpha_1 = 0.5$ a second-order code coupling scheme in time is obtained.

This algorithm was introduced by Farhat et al. (1995) and Farhat and Lesoinne (1997). It provides good results for aero-elasticity problems, such as flow past panel flutter (Piperno et al., 1995; Piperno, 1997). However, from a computational point of view, as far as boundary conditions are concerned, this choice makes it more difficult to satisfy the geometric conservation law at the interface (Thomas and Lombard, 1979).

2.2.2. Explicit asynchronous algorithm (EAA)

With an asynchronous code-coupling scheme, fluid and structure problems are not solved at the same time. Fluid computation is expressed at time $t^{n+1/2}$ and structure computation at time t^{n+1}, as depicted in Fig. 2(b).

The following prediction of first order is used for the fluid mesh displacement:

$$X_m^{n+1/2} = X_s^n + \frac{dt}{2} V_s^n. \tag{10}$$

Then the fluid forces are computed at time t^{n+1}. This procedure ensures a better geometry mesh conservation. It also guarantees the continuity of the displacement and the velocity at the fluid–structure interface according to the Geometric Conservation Law (Thomas and Lombard, 1979). For example, by using the previous Newmark structure

solver algorithm and the trapezoidal rule, the energy conservation property is deduced from

$$V_m^n = \frac{X_m^{n+1/2} - X_m^{n-1/2}}{dt} = \frac{X_s^n - X_s^{n-1}}{dt} + \frac{V_s^n - V_s^{n-1}}{2} = V_s^n, \tag{11}$$

where V_m^n is the mesh velocity at time t^n.

2.2.3. Implicit algorithm (IA)

An implicit code coupling scheme is also possible by using a partitioned method at each time step, based on Newton's or fixed point algorithms (Hermann and Steindorf, 1999; Le Tallec and Mouro, 2001; Mani, 2003; Abouri et al., 2003).

This algorithm uses convergent explicit predictions of the coupled fluid structure system (Fig. 2(c)). Subcycling is involved to get convergence for each subsystem. A criterion based on the fluid force or on the structure velocity is used at each time step to stop the numerical subcycling process.

The computational procedure is described as follows. A reference state at time t^n is defined for the fluid, for the velocity, the pressure and the mesh, and also for the structure, for the displacement, the velocity and the acceleration. For the computation of fluid and structure variables at step t^{n+1}, each time step consists of the following subcycling (referred to as k):

(i) fluid force computation $(F_f^{n+1})^0$ in terms of F_f^n,
(ii) prediction of structure displacement $(X_s^{n+1})^k$,
(iii) deformation of current geometry $(\Omega_f^{n+1})^k$,
(iv) determination of new geometry $(\Omega_f^{n+1})^{k+1}$ and forces $(f_f^{n+1})^{k+1}$,
(v) calculation of error estimator: $\varepsilon = |(F_f^{n+1})^{k+1} - (F_f^{n+1})^k|/|(F_f^{n+1})^0|$.

If the error estimator is lower than a critical value, the next time step t^{n+2} is incremented. Otherwise, the process restarts from the initial state t^n and the last velocity estimation $(X_s^{n+1})^k$ is used for the next subcycling of this algorithm. This reiterative process is based on a fixed point method and it is stable. It is of first-order and it can be improved by using a higher-order algorithm like a Newton's method (Abouri et al., 2003) or a conjugate gradient method (Daim et al., 2002). In order to keep the code-coupling algorithm properties, sufficiently high-order time integration solvers must be used for fluid and structure computations.

To illustrate the property of the previously mentioned explicit and implicit code coupling schemes (ESA, EAA, IA), several test cases are investigated below. Scheme properties are discussed in terms of energy conservation for a simplified test case (Bendjeddou, 2005) and for more complex configurations and in each case, comparisons to analytical solutions are performed.

2.3. Scheme properties

2.3.1. Basic test case

In this part an one-dimensional test case is considered. It involves two structures, each of them being represented by a mass point (referred to as M_1 and M_2). They are linked by a spring with a stiffness K_s and no damping (Fig. 3). The system satisfies the mass spring equations

$$M_1 \frac{d^2 X_s^1}{dt^2} + K_s X_s^1 = K_s X_s^2, \quad M_2 \frac{d^2 X_s^2}{dt^2} + K_s X_s^2 = K_s X_s^1, \tag{12,13}$$

where X_1 and X_2 designate the displacement of each structure.

This basic example consists of a mass spring system and gives a simplified representation of a fluid–structure interaction system. Eq. (12) can be seen as the representation of a single structure problem where the right-hand side corresponds to the loading exerted by fluid forces. Eq. (13) can be considered as the fluid problem providing an estimation of the loading incorporated into Eq. (12).

Fig. 3. One-dimensional test case involving two mass points linked by a spring with a stiffness and without structural damping.

The following initial conditions on the initial structure displacements X_1, X_2 and velocities V_1, V_2 are imposed:

$$X_1(0) = X_0 = -2X_2(0), \quad V_2(0) = V_1(0) = 0, \tag{14,15}$$

where X_0 is a constant.

With the additional condition: $M_2 = M_1/2$, an analytical solution is given by

$$X_s^1(t) = X_0 \cos(2\pi f t), \quad X_s^2(t) = -2X_s^1(t), \tag{16,17}$$

where $2\pi f = \sqrt{3K_s/M_1}$ designates the system circular frequency and X_0 is the displacement magnitude.

Time step sensitivity analysis of this mass spring system has been carried out to estimate energy conservation and numerical stability of coupling schemes. A Newmark method is used for time integration in order to solve each equation. Since both models have only one degree of freedom, each equation is obviously solved implicitly. Different time steps have been used to compare the three time integration schemes previously mentioned. In Fig. 4, the relative error on the energy of the system defined by $(E(t)-E_0)/E_0$ is plotted. E_0 and $E(t)$ are defined by

$$E_0 = \tfrac{1}{2}K_s(X_1(0) - X_2(0))^2, \tag{18}$$

$$E(t) = \tfrac{1}{2}K_s(X_1(t) - X_2(t))^2 + \tfrac{1}{2}M_1V_1(t)^2 + \tfrac{1}{2}M_2V_2(t)^2. \tag{19}$$

As expected, the implicit time integration scheme satisfies better the total energy conservation than the two explicit methods to be tested. The violation of the energy conservation for the two explicit methods, ESA and EAA, is due to the explicit coupled computation of Eqs. (12) and (13). At each time step, both equations are implicitly solved by using

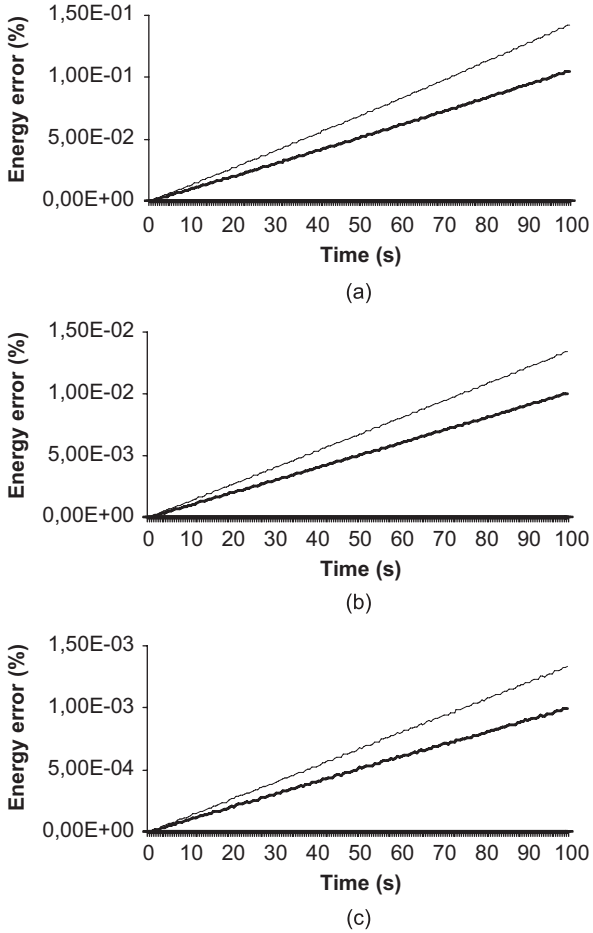

Fig. 4. Comparison of the energy relative error for: (a) $dt = 10^{-3}$ s, (b) $dt = 10^{-4}$ s, (c) $dt = 10^{-5}$ s; ▬, with implicit scheme; ▬, explicit asynchronous scheme; —, explicit synchronous scheme.

an acceleration algorithm, called a-form of Newmark method (with parameters $\beta = 1/2$ and $\gamma = 1/2$), where a prediction step for the computation of $\tilde{X}_i^{n+1}$ and $\tilde{V}_i^{n+1}$ (with $i = 1$ or 2) is followed by a correction step for A^{n+1}, X^{n+1} and V^{n+1}. For the prediction step, this leads to

$$\tilde{X}_i^{n+1} = X_i^n + dt\, V_i^n + \tfrac{1}{2}dt^2(1-2\beta)A_i^n, \tag{20}$$

$$\tilde{V}_i^{n+1} = V_i^n + (1-\gamma)\, dt\, A_i^n, \tag{21}$$

where dt designates the current time step. In the present work, the same time step is used for the two systems. For each equation i, the following system is solved implicitly:

$$(M_i + \beta\, dt^2\, K_s)A_i^{n+1} = F_i^{n+1} - K_s\tilde{X}_i^{n+1}. \tag{22}$$

Then the correction step is

$$X_i^{n+1} = \tilde{X}_i^{n+1} + \beta\, dt^2\, A_i^{n+1}, \tag{23}$$

$$V_i^{n+1} = \tilde{V}_i^{n+1} + \gamma\, dt\, A_i^{n+1}. \tag{24}$$

This basic example illustrates the energy dissipation produced by an explicit direct method. Total energy error is plotted for different time steps in Fig. 4. Energy dissipation decreases with smaller time steps. With an explicit asynchronous scheme, the energy error is 30–40% smaller than the energy error generated by an explicit synchronous scheme.

2.3.2. Interface conditions

In order to study the energy conservation at the interface, the variation of fluid and structure energy respectively ΔE_f and ΔE_s can be estimated under the assumption that the first equation of system (Eq. (12)) provides the structure displacement while the second one (Eq. (13)) gives the fluid forces at the coupling interface. Thus, the fluid forces acting on the structures represent, respectively, $F_f^n = K_s X_1^n$ and $F_s^n = K_s X_2^n$. If an explicit code coupling procedure is involved, the conditions to minimize the numerical energy are deduced from Eq. (8). These extrapolations are not necessary with an implicit code coupling scheme because fluid forces are predicted by successive subcycling iterations in the fluid computation.

2.3.3. Energy conservation

In what follows, a comparison is made of the energy conservation properties of ESA, EAA and IA by using the previously mentioned one-dimensional test case. Results in terms of force and displacement, frequency and damping are deduced from suitable post-processing methods.

As far as code coupling is concerned, specific attention must be paid to energy conservation at the coupling interface. The mass spring problem is solved by using different algorithms. It is shown that fluid and structure energy variations are reduced by using scheme ESA or scheme IA, as illustrated in Fig. 4. The energy conservation properties of the three methods are compared. Numerical damping is lower with the implicit algorithm which has the advantage of preserving equilibrium between the fluid and structure at each time step. Comparing the two explicit methods, the EAA features a better energy conservation than the ESA. This improvement produced by a staggered advancement in time has already been pointed out (Farhat and Lesoinne, 1997). Different time steps have been tested for this specific simple problem involving a mass-spring system. Energy dissipation is limited with the explicit synchronous algorithm and the two explicit methods converge to the solution given by the implicit method.

Furthermore errors between analytical and numerical solutions are compared for the three code coupling schemes ESA, EAA and IA. Schemes ESA and IA provide the best results and the error increases slowly in time. The explicit synchronous scheme cannot satisfy in the same time velocity and displacement continuity and it leads to numerical errors polluting the numerical simulation. One can conclude that numerical damping created by implicit or explicit asynchronous code coupling schemes is lower than damping generated by an explicit synchronous scheme. Besides a comparison with a fully implicit monolithic procedure by using a fluid–structure finite element code is achieved in Table 1. The two masses and the spring are modelled as two discrete finite elements and a linear element. As shown for the partitioned implicit code coupling scheme, the monolithic procedure provides good results in terms of numerical damping. A fully implicit monolithic process involves a strong coupling solver.

Table 1
Comparison of analytical and numerical solutions obtained for explicit synchronous, asynchronous and implicit schemes, with structure mass $M_2 = \frac{1}{2}M_1$, structure stiffness $K_s = K_1 = K_2$ and no damping, for time step $dt = 10^{-5}$ s

Basic test case	Error on frequency	Error on damping
Explicit synchronous	7.1×10^{-5}	8.7×10^{-5}
Explicit asynchronous	5.4×10^{-5}	6.9×10^{-6}
Implicit	1.9×10^{-5}	9.0×10^{-12}
Analytical solution	0.0	0.0

3. Test simulation and validation

In the previous section, methods for code coupling have been discussed and standard schemes have been compared in terms of accuracy and stability at the interface where the coupling is involved. In the present part, these methods are tested on realistic test cases in order to evaluate them when applied to interesting configurations involving tubes and tube bundles in the presence of quiescent fluid or flow. Numerical solutions are compared to available experimental or analytical data.

3.1. Numerical versus analytical solutions

3.1.1. Fluid force identification

Numerical simulation of structure flow-induced vibrations requires fluid force identification. In this section, methods for identification of fluid structure forces are described. In the framework of classical formulations, the structure dynamic equation in a fluid at rest can be written as follows:

$$M_s A_s + C_s V_s + K_s X_s = F = F_c + F_t = -M_a A_s - C_a V_s + F_t. \tag{25}$$

In this expression, M_a and C_a designate, respectively, mass and damping added by the presence of the fluid around the structure. The fluid force referred to as $F_c = -M_a A_s - C_a V_s$ corresponds to the fluid–structure force generated by the coupling between fluid and structure motions at the fluid structure interface. The remaining term, F_t, designates fluid forces independent of the structure motion. For laminar flows, this term is assumed to be zero.

Numerical methods for identification of fluid–structure parameters M_a and C_a are presented below and rely on convenient data processing. Estimation of added mass and damping in fluid at rest in specific configurations is discussed below. First the fluid forces identification method is described. Then results of studies carried out on two test cases are presented, finally conclusions on the performance of the methodology are discussed. In each case, a threshold of convergence has been chosen, but one could improve the results with a convergence in mesh or by using a Richardson convergence procedure (Richardson, 1910).

3.1.2. Inviscid fluid test case

The identification of fluid–structure forces induced by a rigid, undamped moving tube surrounded by an inviscid fluid at rest and a fixed tube is investigated in the present part. The configuration is depicted in Fig. 5.

The purpose is to focus on the global energy conservation of the fully coupled fluid–structure system. The numerical model is presented and finally both analytical and numerical results are compared (Bendjeddou, 2005). Fluid and structure characteristics are presented in Table 1. In this problem, the fluid is considered at rest which makes the fluid motion initialization possible. One considers an initial internal tube displacement with an amplitude $X_0 = 10^{-2}$ mm. Analytical added mass and damping for this test case are deduced from Eqs. (33) and (34). All configuration parameters are reported in Table 2. The expected displacement for a non-damped structure in an inviscid fluid is expressed as follows:

$$X_s = X_0 \cos(2\pi f_c t). \tag{26}$$

The computation is discussed below. The analytical expression is detailed in the appendix.

The tube displacement satisfies the mechanical Eq. (25). In this case, added parameters M_a and C_a are added mass and damping induced by fluid at rest. A fluid–structure code coupling is used to get these coefficients. A second-order time integration solver, a Newmark algorithm for the structure and a Crank–Nicholson algorithm for the fluid are involved. The three code-coupling explicit synchronous, explicit asynchronous and implicit schemes are tested. To get

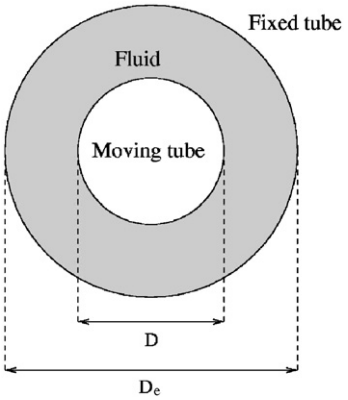

Fig. 5. Configuration of the test case involving two coaxial tubes separated by a fluid initially at rest.

Table 2
Table for fluid and structure properties for the inviscid test case

Non viscous fluid test case parameters	Fluid	Structure
Density	$1000\,\mathrm{kg\,m^{-3}}$	
Dynamic viscosity	0	
Internal tube diameter		2 mm
External tube diameter		2.5–5 mm
Reference length		1 mm
Mass		5.96×10^{-4} kg
Stokes number		∞
Damping		0%
Frequency		119.36 Hz

Table 3
Comparison of analytical and numerical results with explicit synchronous, explicit asynchronous, implicit partitioned and fully implicit coupling schemes with a time step: $dt = 10^{-5}$ s for the inviscid fluid test case with parameters of Table 2

Inviscid fluid test case	Frequency f_c (Hz)	Damping ξ (%)
Explicit synchronous	118.92	0.0331
Explicit asynchronous	118.92	0.0228
Implicit	118.92	0.0032
Fully implicit	119.02	0.0018
Analytical solution	118.93	0

accurate results, second-order time integration solvers, a Newmark one for the structure and a Crank–Nicholson one for the fluid are used. Moreover, in the Crank–Nicholson scheme, the pressure and velocity field computations are staggered in time, pressure is expressed at time $t^{n+1/2}$ and velocity at time t^{n+1}. A linear extrapolation of the pressure at time t^{n+1} is performed in order to compute fluid force acting on the tube,

$$F^{n+1} = \tfrac{3}{2}F^{n+1/2} - \tfrac{1}{2}F^{n-1/2}. \tag{27}$$

Numerical simulation introduces an artificial damping and the tube displacement satisfies the following equation:

$$X_s = X_0\cos(2\pi\tilde{f}_c t)\,\mathrm{e}^{-\tilde{\xi}t}, \tag{28}$$

where $\tilde{f}_c$ and $\tilde{\xi}$ designates, respectively, the numerical frequency and damping to be identified. Errors in tube frequency f_c and damping ξ obtained with the three code-coupling schemes are given in Table 3. As in the one-dimensional test

case, the numerical damping is reduced with the implicit and explicit asynchronous schemes and each scheme gives a good estimation of tube frequency for fluid at rest.

3.1.3. *Viscous fluid test case*

Fluid–structure forces induced by a rigid moving tube surrounded by a viscous fluid initially at rest and a fixed tube are considered (Fig. 5). The configuration parameters are reported in Table 2, except for the Stokes number and the dynamic viscosity. To test several Stokes numbers, one acts on the dynamic viscosity value. It is chosen to be very small for $\mathrm{St} = \infty$. This procedure makes it possible to keep the same solver for inviscid and viscous fluid, a non-zero value of viscosity being necessary to overcome a computational overflow situation. The tube displacement satisfies the classical mechanical Eq. (25). The numerical fluid–structure coupling method introduces a coupling between fluid and structure computations. From an analytical point of view, results can be compared to those obtained with a similar corresponding method. This method requires initial conditions on displacement, velocity and force. Here initial structure displacement X_0 is chosen to start structure displacement with a fluid initially at rest. The reference analytical solution is given in the appendix.

First, numerical displacement obtained with the three code coupling schemes by using the same time step and the same fluid mesh are compared. Table 4 shows that numerical damping introduced by coupling is reduced by using an explicit asynchronous or an implicit code coupling scheme. Errors between numerical and analytical solutions deduced from Eqs. (31) and (32) are reported.

Convergence in time and space for the explicit asynchronous code coupling scheme have been performed. Several meshes with different boundary layer refinements have been used for space convergence. Example of meshes are illustrated in Fig. 6. Results of time convergence tests are depicted in Table 5. Numerical results are in good agreement with analytical solution with less than 5% error. Then the influence of the initial displacement and higher Stokes number on fluid–structure coefficients is pointed out. For all computations, the initial tube displacement is small. It is chosen so that the flow remains laminar. Table 6 shows that there is no significant effect of the initial amplitude on numerical results. The effect is less then 1%. Finally the effect of viscosity is measured. Numerical results for small and large Stokes numbers are in good agreement with analytical solutions (Table 7).

Table 4
Comparison of different code coupling scheme explicit synchronous, explicit asynchronous and implicit schemes with a 896 cells mesh and a $dt = 5 \times 10^{-4}$ s time step for the viscous fluid test case

Viscous fluid test case	Added mass M_a	Added damping C_a
Explicit synchronous	1.22	1266.63
Explicit asynchronous	1.22	759.32
Implicit	1.20	503.69
Analytical solution	1.18	497.20

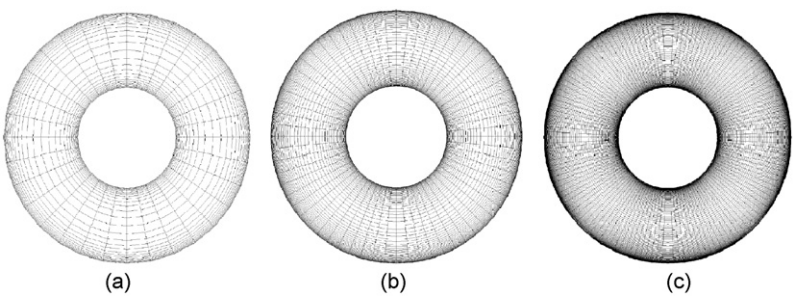

Fig. 6. Examples of meshes used to simulate the coaxial tube test case: (a) coarse (896 cells), (b) middle (3712 cells) and (c) fine meshes (16 048 cells).

Table 5
Time convergence with an asynchronous explicit scheme on a 3712 cells mesh for the viscous fluid test case

Time step (s)	5×10^{-4}	5×10^{-5}	2.5×10^{-5}	1.25×10^{-5}
Added mass M_a	1.19	1.19	1.18	1.18
Added damping C_a	738.83	513.42	500.99	497.60

Table 6
Influence of initial tube displacement X_0 expressed in percent of tube diameter on fluid–structure coefficient with an asynchronous code coupling scheme with a time step $dt = 5\times10^{-5}$ s and a 3712 cell mesh for the viscous fluid test case

Initial amplitude X_0/D (%)	5	1	0.1
Added mass M_a	1.19	1.18	1.18
Added damping C_a	517.09	517.85	518.53

Table 7
Comparison of analytical and numerical results for the viscous fluid test case for two Stokes number values: St = 800 (top) and St = 14 036 (bottom)

	Analytical (–)	Numerical (–)
Stokes number St = 800		
Added mass M_a	1.1790	1.1868
Added damping C_a	497.20	501.10
Stokes number St = 14 036		
Added mass M_a	1.1044	1.1069
Added damping C_a	1989.60	2039.21

3.2. Weak versus strong coupling methods

The next part is devoted to the validation of the fluid-structure coupling tool by using different test cases. The explicit asynchronous scheme is used.

3.2.1. Concentric tubes

Fluid–structure forces induced by a rigid moving tube surrounded by a viscous fluid at rest and a fixed tube is modelled.

A complete analytical and experimental study of this configuration is considered (Chen et al., 1976; Chen, 1987; Yeh and Chen, 1978). Analytical estimations of added mass and viscous damping coefficient are available. The following notations are introduced: D and D_e designate, respectively, the moving and the non-moving tube diameters. Different tube diameter ratio values are studied: $D_e/D = 1.2, 2.5, 4, 10$; and in each case, different Stokes number values St are considered: St = 10, 100, 5000, ∞. A space and a time convergence has been achieved. Fixed cells in the tube reference are introduced in the vicinity of the tube in order to avoid near-wall local mesh distortion. Dimensionless added mass and viscous damping estimated numerically are compared to available analytical values in Fig. 7 for several diameter ratios and Stokes numbers. Numerical results are in good agreement with expected solutions and the tube in fluid at rest features the expected behaviour. For Stokes number St = 5000, error on the dimensionless parameters are reported in Table 8. One gets an error smaller than 5% between numerical solution and available analytical data (Sinyavskii et al., 1980).

3.2.2. Eccentric tubes

In this test case, a tube diameter ratio $D_e/D = 2$ configuration is considered and several cylinder eccentricity values are tested by using the values of $e = 0, 0.3, 0.6$. In these simulations, the Reynolds number is imposed at $R_k = 2\pi f D^2/\nu = 50$. The dynamic viscosity ν is chosen in order to satisfy reasonable tube frequency value.

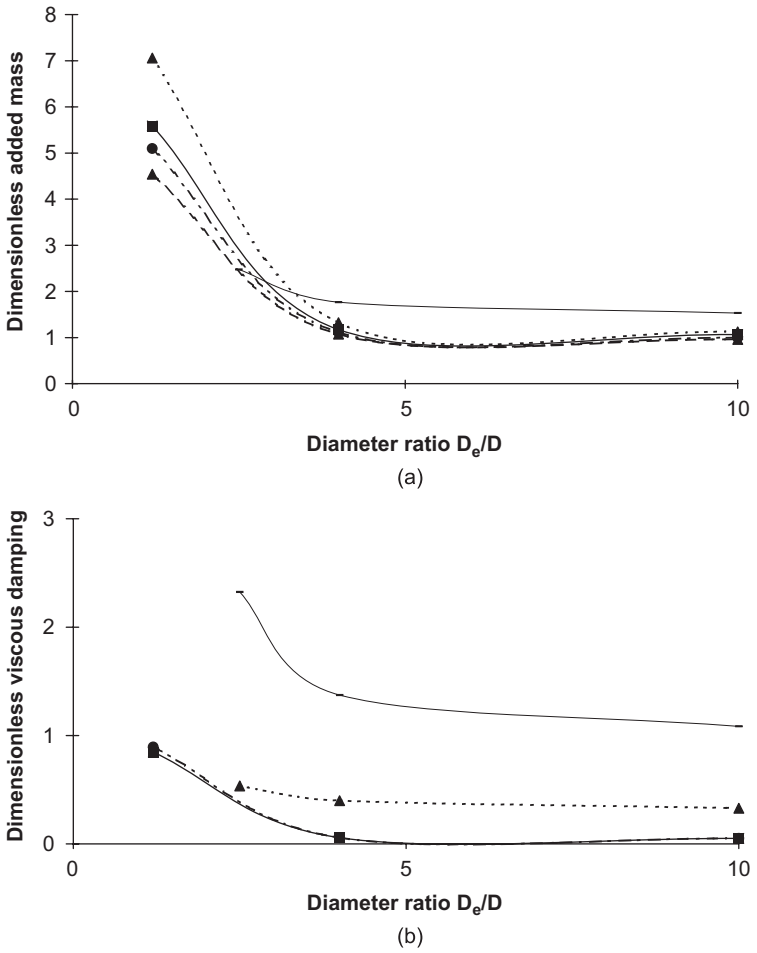

Fig. 7. Evolution of dimensionless added mass and viscous damping coefficients for concentric tubes in terms of diameter ratio and Stokes numbers. (a) Dimensionless added mass, (b) dimensionless viscous damping for viscous fluid: –■–, St = 10; · · ·▲· · ·, St = 100; · · ·●· · ·, St = 5000; ---▲---, for inviscid fluid (infinite Stokes number). For St = 5000: comparison to available analytical solution (–■– line).

Table 8
Error on dimensionless added mass and viscous damping for concentric tube test case with $D_0/D = 4$ and St = 5000

Relative error (%)	Added mass	Viscous damping
Explicit asynchronous	6.65	3.57

In what follows the numerical results obtained with the partitioned procedure are compared to those obtained with an implicit monolithic procedure (Yang and Moran, 1979). The monolithic procedure relies on a finite element method for both fluid and structure computations by using a strong coupling formulation.

An example of mesh used with the partitioned procedure is shown in Fig. 8. Dimensionless added mass and viscous damping are plotted in Fig. 9 for several eccentricity values. Numerical results obtained with the partitioned procedure and with the monolithic one are compared; they are in good agreement. The partitioned scheme provides good results in terms of numerical damping like a fully implicit solver. The mechanical energy of the whole fluid–structure system is expressed for these different code coupling schemes. The mechanical energy is conserved for a inviscid fluid and a non-damped structure. The implicit code coupling scheme ensures better energy conservation.

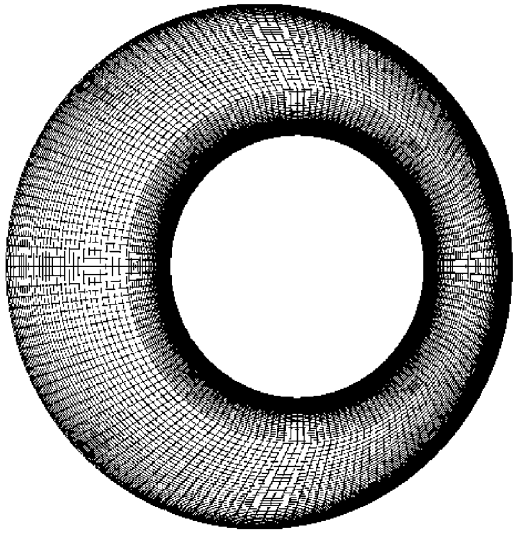

Fig. 8. Example of mesh for the test case involving coaxial tubes with an eccentricity $e = 0.3$.

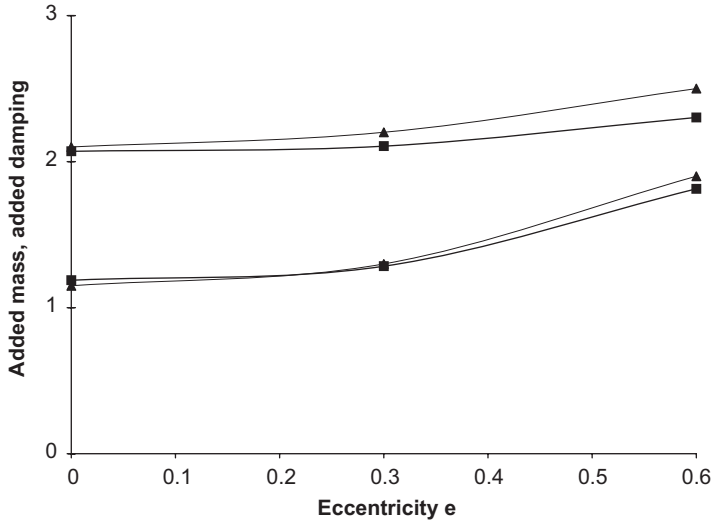

Fig. 9. Evolution of dimensionless added mass and viscous damping coefficients in terms of eccentricity for eccentric tubes. Comparison between numerical solutions obtained with a partitioned procedure and with a monolithic coupling algorithm (Chen, 1987). –■–, partitioned procedure solutions –▲–, monolithic procedure solutions.

3.3. Numerical versus experimental results

3.3.1. Tube bundles test case

A tube bundle configuration is studied and numerical identification of added mass and damping in fluid at rest for a single tube (Fig. 10) moving in a fixed tube array is investigated. The configuration is an in line square array with a pitch ratio diameter $P/D = 1.5$ (Weaver and Abd-Rabbo, 1985). Numerical results obtained with the partitioned procedure are compared to available experimental results (Weaver and Abd-Rabbo, 1985). The test case characteristics are given below. The structure frequency in air is $f_s = 25.5\,\text{Hz} \pm 0.2\,\text{Hz}$, the Stokes number is: $\text{St} = f_s D^2/\nu = 16\,000$ and the structure damping values in air and in still water are given by the following logarithmic decrements: $\delta_s = 0.014 \pm 0.001$ and $\delta_e = 0.037 \pm 0.004$.

One fixes the structure frequency and chooses a mass to find the structure stiffness, then selects the structure damping in order to get a logarithmic decrease in air.

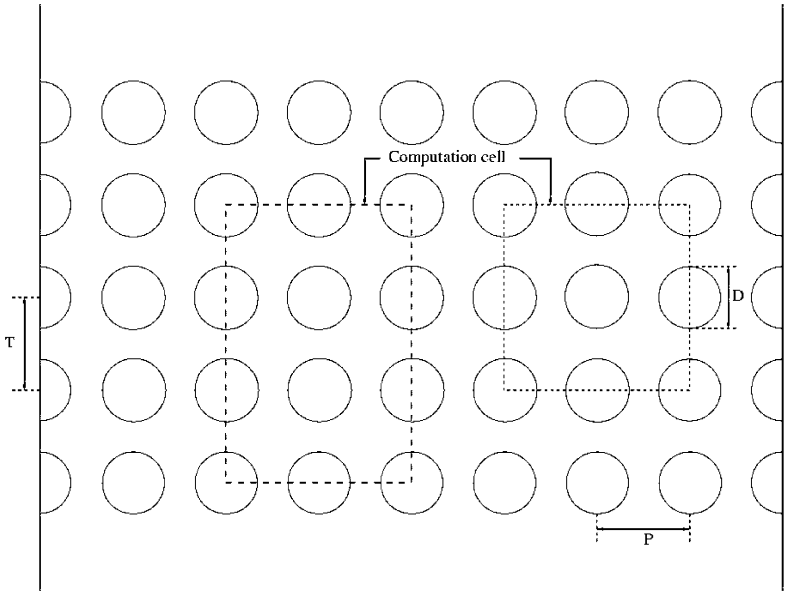

Fig. 10. Configuration for the test case involving a tube bundle with a pitch ratio of $P/D = 1.5$ (Weaver and Abd-Rabbo, 1985).

Table 9
Error on frequency and added damping estimated numerically for the tube array test case with pitch ratio $P/D = 1.5$

Relative error (%)	Frequency	Viscous damping
9-tube model	3.89	6.16
12-tube model	1.23	3.64

In what follows the added damping estimated numerically and logarithmic decrement in water for measuring the added damping are compared. Fluid–structure coefficients depend only on the Stokes number and tube confinement. Structure mass and stiffness in air could be chosen arbitrarily and have to satisfy the given structure frequency in air.

In this computation, the fluid is Newtonian and the flow is two-dimensional and incompressible. Periodic boundary conditions are used on elementary 9-tubes and 12-tubes computational cells in order to simulate an infinite tube bundle. The explicit asynchronous code coupling scheme is used. By using an empirical law (Rogers et al., 1984), one can find the added mass and damping. This law allows to make the correspondence between a tube bundle (with a pitch ratio diameter given) and two coaxial tubes (with a diameter ratio) for the fluid-structure coefficients.

These values, associated to the structure mass and damping, will enable us to find the analytical logarithmic decrement in water δ_{theo}, and the analytical frequency f_{theo}, found by using the structure frequency. The error of different numerical results are compared in Table 9. As an indication, one can use the experimental results for the added damping $\delta = 0.037 \pm 0.004$.

Numerical results are in good agreement with experimental measurements, with an error smaller than 10%.

4. Conclusion

Nowadays, code-coupling methods are possible for solving complex fluid–structure interaction problems. This technique features great flexibility and modularity: a fluid dynamics code and a structural dynamics code can be coupled by using an efficient coupling interface. This method takes advantage of the parallel process involved within each analysis code. This allows both parts of the fluid–structure interaction problem to be solved in the best possible way, for example a Finite Volume Method for the fluid dynamics and a Finite Element Method for the structure.

Depending on the generality of the two codes, complex flows and structure motions can be considered and their coupling successfully modelled. The only requirement consists in creating routines to exchange suitable information between the two solvers. Unfortunately, due to the explicit nature of this coupling, convergence problems may occur. Consequently, there is a restriction on the time step even if implicit time integration schemes are used by both solvers.

The coupled fluid–structure or monolithic algorithm requires reformulation of the equations and it implies restrictions on the choice of the numerical methods to be used. However, as far as time advancement is concerned, because of the simultaneous solution of both parts of the fluid–structure problem, there is no approximation error due to data transfer at the interface, and no time-step restriction for stability. Therefore the monolithic method can be used with large time steps, but it is more difficult to implement than the partitioned procedure. The linear system of the coupled problem may have a high conditioning parameter number if fluid and structure dynamics are solved in different scales, which may create a wide spectrum in the coupled linear system. The convergence properties of the coupling method can be improved by exchanging the data at the interface between the fluid and structure several times per time step, which is the case of the implicit method presented in this paper. With regard to stability condition, the implicit method can be used with larger time steps. This is not the case for the two explicit methods considered in this article. The implicit method is widely used and it has been shown to be very efficient for industrial applications. With regard to the energy conservation at the interface, the implicit method satisfies better the required conditions. For further validation of the method, more applications to fluid–structure problems must be investigated. Especially in the framework of industrial configurations involving complex flows around vibrating tubes, this work is particularly valuable.

Appendix A. Analytical expression for the coaxial tube test case

As far as tube and tube bundle vibrations are concerned, analytical expressions of fluid–structure parameters—the added mass and damping M_a and C_a as formulated in Eq. (25)—can be based on the theory and assumptions described by Chen (1987). Sinyavskii et al. (1980) developed the following equivalent expression for M_a and C_a:

$$M_a = \rho\pi\frac{D^2}{4}L\left(\frac{D_e^2+D^2}{D_e^2-D^2}+\frac{4}{D}\left(\frac{\nu}{\pi f}\right)^{1/2}\right) \tag{29}$$

and

$$C_a = \frac{2\pi\mu D}{\sqrt{\nu/\pi f}}L\left[\frac{D_e^4+D^3D_e}{(D_e^2-D^2)^2}\right], \tag{30}$$

where ρ, μ, ν, D, L designate, respectively, fluid density, fluid viscosities, tube diameter and length in the tube direction.

For high Stokes number, the latest formula of added mass and viscous damping (29) and (30) are equivalent to the following expressions:

$$M_a = \rho D^2 L\left(\frac{\pi}{4}\frac{[1+(D/D_e)^2]}{[1-(D/D_e)^2]}+\sqrt{\frac{\pi}{\mathrm{St}}}\right), \tag{31}$$

$$C_a = \mu L\left(2\pi^{3/2}\sqrt{\frac{\rho f D^2}{\mu}}\frac{1+(D/D_e)^3}{(1-(D/D_e)^2)^2}\right) \tag{32}$$

if the following condition is satisfied:

$$\mathrm{St} = \pi f D^2/2\nu \gg 1.$$

This formulation has been developed (Sinyavskii et al., 1980; Chen, 1987) for high Stokes numbers.

When the fluid tends to be inviscid (with dynamic viscosity $\mu = 0$), the associated Stokes number satisfies $\mathrm{St} = (\rho f D^2/\mu) = \infty$, and the previous expressions simplify to

$$M_a \simeq \rho D^2 L\left(\frac{\pi}{4}\frac{[1+(D/D_e)^2]}{[1-(D/D_e)^2]}\right), \quad C_a \simeq 0. \tag{33,34}$$

References

Abouri, D., Parry, A., Hamdouni, A., 2003. Fluid/rigid body interaction in complex industrial flow. Chapter–Advances in fluid mechanics. In: Fluid Structure Interaction II. WIT Press, Cadiz, Spain, pp. 295–305.

Bendjeddou, Z., 2005. Numerical simulation of flow induced vibration in tube bundles. Ph.D. Thesis, Lille University, France.

Chen, S.S., 1987. Flow induced vibration of circular cylindrical structures. Hemisphere Publishing Corporation, New York, USA.

Chen, S.S., Wambsganss, M.W., Jendrzejczyk, J.A., 1976. Added mass and damping of a vibrating rod in confined viscous fluids. Journal of Applied Mechanics 43, 325–329.

Daim, F., Eymard, E., Hilhorst, D., Mainguy, M., Masson, R., 2002. A preconditioned conjugate gradient based algorithm for coupling geomechanical–reservoir simulation. Oil and Gas Science and Technology—Review IFP 57 (5), 515–523.

Farhat, C., Lesoinne, M., 1997. Improved staggered algorithms for the serial and parallel solution of three-dimensional nonlinear transient aeroelastic problems. Center for Aerospace Structures—97–11, University of Colorado, Boulder, Colorado. In review in AIAA Journal.

Farhat, C., Lesoinne, M., Maman, N., 1995. Mixed explicit implicit time integration of coupled aeroelastic problems: three field formulation, geometric conservation and distribution solution. International Journal for Numerical Methods in Fluids 21, 807–835.

Hermann, G.M., Steindorf, J., 1999. Efficient partitioned procedures for computation of fluid structure interaction on parallel computers. In: Developments in Computational Mechanics with High Performance Computing. Civil-Comp Press, Edinburgh, S, pp. 127–136.

Hughes, T.J.R., Liu, W.K., Zimmerman, T.K., 1981. Lagrangian Eulerian finite element formulation for viscous flows. Computational Methods for Applied Mechanical Engineering 29, 329–349.

Le Tallec, P., Mouro, J., 2001. Fluid structure interaction with large structural displacement. Computational Methods for Applied Mechanical Engineering 190, 3039–3067.

Longatte, E., Bendjeddou, Z., Souli, M., 2003. Methods for numerical study of tube bundle vibrations in cross-flows. Journal of Fluids and Structures 18, 513–528.

Mani, S., 2003. Truncation error and energy conservation for fluid structure interactions. Computational Methods for Applied Mechanical Engineering 192, 4769–4804.

Morand, H.J.-P., Ohayon, R., 1995. Fluid Structure Interaction. Wiley, Chisester.

Piperno, S., 1997. Explicit/implicit fluid/structure staggered procedures with a structure predictor and fluid subcycling for 2d inviscid aeroelastic simulations. International Journal of Numerical Methods in Fluids 25, 1207–1226.

Piperno, S., Farhat, C., 2001. Partitioned procedures for the transient solution of coupled aeroelastic problems. Part II: Energy transfer analysis and three-dimensional applications. Computational Methods for Applied Mechanical Engineering 190, 3147–3170.

Piperno, S., Farhat, C., Larrouturou, B., 1995. Partitioned procedures for the transient solution of coupled aeroelastic problems. Part I: Model problem, theory and two-dimensional application. Computational Methods for Applied Mechanical Engineering 124, 79–112.

Richardson, L.F., 1910. The approximated arithmetical solution by finite differences of physical problems involving differential equations, with an application to the stresses in a masonry dam. Philosophical Transactions of the Royal Society of London, Series A 210, 307–357.

Rogers, R.J., Taylor, C., Pettigrew, M.J., 1984. Fluid effects on multi-span heat-exchanger tube vibration. In: Pressure Vessel and Piping Conference, San Antonio, TX, USA.

Sinyavskii, V.F., Fedotovskii, V.S., Kukhtin, A.B., 1980. Oscillating of a cylinder in a viscous fluid. Prikladanaya Mekhanika 16 (1), 27–62.

Souli, M., Zolesio, J.P., 2001. Arbitrary Lagrangian–Eulerian and free surface methods in fluid mechanics. Computational Methods for Applied Mechanical Engineering 191, 451–466.

Thomas, P.D., Lombard, C.K., 1979. Geometric conservation law and its application to flow computations on moving grids. AIAA Journal 17, 1030–1037.

Weaver, D.S., Abd-Rabbo, A., 1985. A flow visualisation study of a square array of tubes in water crossflow. ASME Journal of Fluids Engineering 107, 354–363.

Yang, C.I., Moran, T.J., 1979. Finite-element solution of added mass and damping of oscillation rods in viscous fluids. Journal of Applied Mechanics 46, 519–523.

Yeh, T.T., Chen, S.S., 1978. The effect of fluid viscosity on coupled tube/fluid vibration. Journal of Sound and Vibration 59 (3), 453–467.